International Journal of ChemTech Research
CODEN (USA): IJCRGG ISSN: 0974-4290
Vol.7, No.5, pp 2448-2453, 2014-2015

# An XRD study on Zn-doped forsterite nanoparticle at two different treating temperatures

**B. Karthikeyan[1]*, K. Balachandrakumar[1], and N. Rajamanickam[2]**

[1]Department of Physics, Kamaraj College of Engineering and Technology, Virudhunagar – 626 001, India
[2]Physics Research Centre, VHNSN College, Virudhunagar – 626 001, India

**Abstract:** The presence of forsterite nanoparticle may be the reason for observing extended red emission (ERE) in many dusty astrophysical environment like our solar system, interstellar medium (ISM), nebulae, etc. Forsterite in nanocrystalline form is one of the important bio-ceramic materials whose mechanical properties are far better than other bio-compatible materials. In view of such astrophysical and biomedical applications, the present work is focused on the synthesis and characterization of un-doped and doped forsterite in nanocrystalline form. The pure and Zn-doped forsterite nanoparticle were therefore synthesized using the mixture of talc, periclase and the oxide of doping element (Zn) through a mechanical activation method followed by heat treatment at $850^0$C / $1000^0$ C for 1 hour. The prepared samples were analyzed using XRD technique. The results of XRD indicate that the particle size has been significantly varying from 40 nm to 50 nm due to the addition of impurities into the pure form of forsterite. Morphology index, strain, Lorentz factor and Lorentz-Polarization factor have also been evaluated and discussed.
**Keywords:** Zn-doped forsterite; Synthesis; XRD analysis; Astrophysical significance.

## Introduction:

In recent years, nanoscience and nanotechnology has become very popular in all the fields of research. There are various techniques to synthesize nanomaterials such as inert gas condensation, chemical vapor deposition, plasma arcing, electro-deposition, sol-gel, high energy ball milling, etc. [1-2]. Among these methods, high energy ball milling has advantages of being simple, relatively inexpensive and applicable to any class of materials and can be easily scaled up to large quantities [3]. Ball milling induces self-sustaining reactions in many sufficiently exothermic powder mixtures and the chemical reactions induced by milling or mechanical treatment are known to be very effective for the preparation of nanocrystalline powders consisting of more than two phases [4]. In the present work, the ball milling is therefore adopted for the synthesis of our samples.

Forsterite is a crystalline magnesium silicate having the chemical formula $Mg_2SiO_4$. It plays a vital role in many fields like electronics, biomedical engineering, astrophysics, etc. Featuring low microwave loss and extremely low electrical conductivity, forsterite can be used in electron tubes and as a substrate material in electronics [5]. The rigorous oxidation-reduction environment stability, excellent electrical insulation and high heat endurance up to $1700^0$C) make forsterite a preferable material for the production of gaskets in solid-oxide fuel cell [6]. Forsterite can act as a potential biomaterial for prosthetic implants because of its higher fracture toughness [7]. Kioke *et al* [8] suggested that thermo-luminescence spectra of forsterite after gamma ray irradiation were very similar to Extended Red Emission (ERE) of Red rectangle, a biconical nebula centered around a post-AGB star.

Because of various significances of forsterite, forsterite has been chosen in the present study. In searching the literature, no information was found regarding the crystallographic properties or characteristics of Zn-doped forsterite except the articles which discussed only the pure form along with other dopants like Cr and Ti. In this paper, we report the effect of doping on the structural properties of forsterite nanoparticle using the mechanical activation method followed by thermal treatment at different concentration of Zn. The prepared mixtures or samples have been characterized by X-ray diffraction (XRD) pattern.

## Experimental and evaluation procedure:

Nanocrystalline pure and Zn-doped forsterite powders were synthesized with the help of a planetary ball mill (Retsch – PM100). The starting materials were talc (99% purity, Sigma Aldrich) and periclase (99% purity, Sigma Aldrich) for getting pure form of forsterite and were mixed in the ratio 1:5 (Mixture 1). For doping Zn into forsterite, the oxide powder of doping element was added with talc and periclase in two different dopant concentrations as mentioned in table-1 (Mixture 2-4). The milling was performed for 3 hours with ball-to-powder weight ratio 9:1. After milling, heat treatment was done at two different temperatures $850^0$C and $1000^0$C for 1 hour using muffle furnace.

**Table-1: Details of different mixtures**

| Mixture | Dopant concentration (in molar ratio) | Annealing temperature ($^0$C) |
|---|---|---|
| 1 | --- | 850 |
| 2 | 15 % | 850 |
| 3 | 25 % | 850 |
| 4 | 15 % | 1000 |

The prepared samples were examined by XRD analysis using PANalytical X'Pert PRO by allowing the Cu-$K_{alpha}$ beam of wavelength of 1.5406 $A^0$. The crystallite size (D) was determined from full-width at half-maximum (FWHM) of XRD peaks using Scherrer's equation

$$D=\frac{0.9\lambda}{\beta Cos\theta} \qquad (1)$$

where λ is the wavelength of incident radiation, β is sFWHM and θ is diffracting angle and their values have been given in table-2.

**Table-2: Particle size and Strain**

| Mixture | Particle Size D (nm) | Strain ε (no unit) |
|---|---|---|
| 1 | 40.90 | 0.008 |
| 2 | 41.58 | 0.007 |
| 3 | 49.45 | 0.006 |
| 4 | 49.13 | 0.006 |

In addition to the calculation of particle size, few more parameters have been deduced using XRD pattern. i.e., Micro strain (ε) was also calculated for the synthesized samples using William-Hall method [9] i.e., by plotting the graph in between $\beta Cos\theta$ and $Sin\theta$. The strain has been obtained from the slope of the linear fit and given in the table-2.

In general, the morphological studies are done using Scanning Electron Microscope (SEM) image. However, it can be done even with the help of XRD pattern to some extent as follows. Morphology index (MI) was evaluated here using the equation [10]

$$MI=\frac{FWHM_h}{FWHM_h + FWHM_p}$$

(2)

where $FWHM_h$ is the highest FWHM value obtained from peaks and $FWHM_P$ is particular peak's FWHM for which MI is to calculated. The derived data for mixtures 1 and 4 only are presented in table-3 and 4 to avoid the extended length of the article and the data for other mixtures may be provided on the readers' request.

**Table-3: Morphology Index, Lorentz factor and Lorentz polarization factor for Mixture 1**

| 2 Theta (deg) | FWHM (Rad) | Particle size (nm) | MI | LF | LPF |
|---|---|---|---|---|---|
| 22.85 | 0.0038 | 96.33 | 0.820 | 0.726 | 4.146 |
| 25.5 | 0.0070 | 22.44 | 0.714 | 7.626 | 57.077 |
| 29.8 | 0.0175 | 12.77 | 0.500 | 0.692 | 2.775 |
| 32.29 | 0.0042 | 40.58 | 0.806 | 1.540 | 8.698 |
| 35.7 | 0.0033 | 85.89 | 0.840 | 0.653 | 3.064 |
| 36.5 | 0.0051 | 36.85 | 0.775 | 0.951 | 4.306 |
| 39.68 | 0.0021 | 134.10 | 0.893 | 0.652 | 3.022 |
| 57 | 0.0175 | 9.05 | 0.500 | 5.123 | 37.087 |
| 58.9 | 0.0175 | 22.92 | 0.500 | 0.762 | 4.560 |
| 62.18 | 0.0070 | 23.28 | 0.714 | 2.574 | 16.803 |
| 67 | 0.0175 | 17.97 | 0.500 | 0.671 | 3.403 |
| 69.6 | 0.0070 | 22.72 | 0.714 | 4.467 | 31.852 |
| 75 | 0.0175 | 90.01 | 0.500 | 6.519 | 48.228 |
| 79 | 0.0175 | 38.69 | 0.500 | 1.156 | 8.338 |
| **Average** | | **40.90** | | | |

**Table-4: Morphology Index, Lorentz factor and Lorentz polarization factor for Mixture 4**

| 2 Theta (deg) | FWHM (Rad) | Particle size (nm) | MI | LF | LPF |
|---|---|---|---|---|---|
| 23.87 | 0.0035 | 54.65 | 0.833 | 0.889 | 3.883 |
| 25.54 | 0.0052 | 30.03 | 0.769 | 6.242 | 46.020 |
| 32.35 | 0.0038 | 44.92 | 0.820 | 1.381 | 7.478 |
| 35.74 | 0.0035 | 79.15 | 0.833 | 0.651 | 2.976 |
| 36.53 | 0.0031 | 58.78 | 0.847 | 0.984 | 4.540 |
| 39.69 | 0.0026 | 108.11 | 0.870 | 0.653 | 3.045 |
| 41.82 | 0.0035 | 93.80 | 0.833 | 0.683 | 3.579 |
| 54.96 | 0.0035 | 62.96 | 0.833 | 0.701 | 2.805 |
| 62 | 0.0175 | 9.65 | 0.500 | 1.674 | 9.734 |
| 62.78 | 0.0033 | 46.46 | 0.840 | 7.130 | 73.039 |
| 67 | 0.0087 | 35.94 | 0.667 | 0.671 | 3.403 |
| 70 | 0.0175 | 9.76 | 0.500 | 1.509 | 8.456 |
| Average | | 49.13 | | | |

It is known that the intensity of XRD peak depend on many factors in which Lorentz factor (LF) and Lorentz-polarization factor (LPF) are so important. Here, they have been evaluated using the equations (3) and (4) [10].

$$LF=\frac{Cos\theta}{Sin^2 2\theta} \quad (3)$$

$$LPF=\frac{1+(Cos^2 2\theta)}{Sin^2 2\theta \times Cos\theta} \quad (4)$$

The obtained LF and LPF values for the mixtures 1 and 4 have been tabulated in table-3 and 4.

## Results and discussion:

Figures from 1 to 4 show the XRD pattern of forsterite and Zn-doped forsterite with different Zn concentration and at two different annealing temperatures $850^0$C and $1000^0$C. In figure 1, several peaks corresponding to the planes (211), (131), (222), (400), (221), etc., of forsterite have been indexed by referring XRD JCPDS data file (no. 34-0189). Additionally, a strong periclase XRD peak and few weak lines of enstatite $Mg_2SiO_3$ are appeared on XRD pattern. However, the periclase peak has been reduced drastically by adding impurity (refer figure 2).

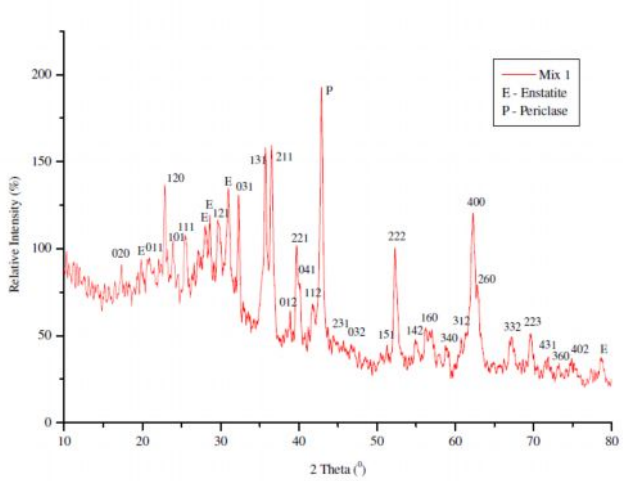


**Figure-1: XRD pattern of Mixture 1 (Undoped)**

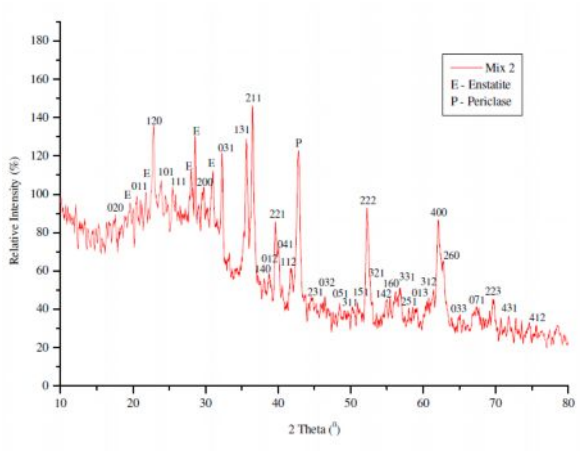


**Figure-2: XRD pattern of Mixture 2 (15% of Zn; 8500C)**

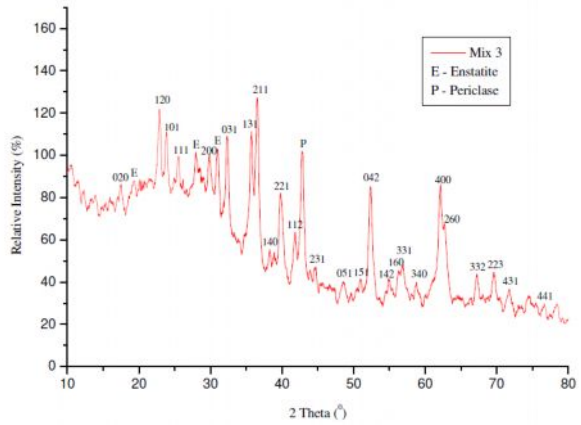


**Figure-3: XRD pattern of Mixture 3 (25% of Zn; 8500C)**

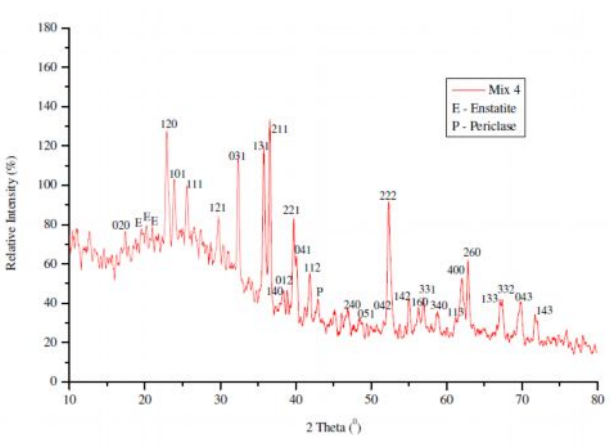


**Figure-4: XRD pattern of Mixture 4 (15% of Zn; 10000C)**

This clearly shows that Zn atom has successfully occupied M1 site of forsterite without changing the orthorhombic structure and the forsterite phase can be increased with reduced periclase and enstatite phases, by adding the impurity Zn. However, there is a constraint that according to Gualtien and Bagni [11], a partial solid solution was observed for Zinc in forsterite and in fact, willemite was formed for Zn > 15 mol % by

experiencing a change in its structure. In literature, there is no information regarding the effect of impurity Zn (except the effect of annealing temperature and milling time) on the formation of forsterite phase.

While substituting Zn ions for Mg ions, XRD trace is not showing any extra peak (figure 2, 3 & 4) which may be due to the reason that both ions have very similar ionic radii (0.60 and 0.57 $A^0$ for Mg and Zn respectively). Since there is no extra peak even after the addition of Zn, one can conclude that the as-grown samples are single phase and there is no change in the orthorhombic structure of forsterite.

The average particle sizes for the different mixtures have been estimated using Scherrer equation and are presented in table-2 which shows that there is no considerable change in the particle size with varying doping concentration. Elastic strain obtained from XRD trace reveals that greater the particles size have less value of strain which means that smaller particles have high strain and bigger particles have less strain. Holland and Murtagh [12] reported the upper and lower limits of talc texture. According to them, the talc textures were varying from 100% blocky at (M = 0) to 100% platy at (M = 1) and could be used to numerically distinguish between blocky and platy talcs. Keeping this in mind, MI values have been calculated in the present study. It is also noticed from the results that when the size of the particle increases, MI is also increased. It is known that the overall effect of Lorentz factor is to decrease the intensity of the reflections at intermediate angles compared to those in the forward or backward directions. Referring the tables-3 and 4, one can observe that there are only few XRD peaks whose LF and LPF values are more deviated.

## Conclusion

The pure and Zn doped nanocrystalline forsterite nanoparticles have been successfully synthesized. The particle size, structural properties and surface analysis are studied in a detailed manner. The results of the present study may be useful aid for various applications. For instance, the identification of nanoclusters in astrophysical environment is still a struggling one for an astrophysicist because of lack of experimental data for the nanoparticles. Similar to the identification of diatomic molecules in sunspot using spectroscopic technique [13-14], it is proposed to do the analysis of forsterite nanoparticle towards the identification of forsterite in red rectangular nebula.

## Acknowledgments

The authors thank the management of Kamaraj College of Engineering and Technology for providing the research facilities in their campus.

## References

1. Cao. G., Nanostructures and Nanomaterials – Synthesis, properties and applications, Imperial College Press, USA, 2004, 3-4.
2. Indris. S., Bork. D., Heitjans. P., Nanocrystalline Oxide Ceramics Prepared by High-Energy Ball Milling, Journal of Materials Synthesis and Processing, 2000, 8(3/4), 245-250.
3. Baraton. M.I., Synthesis, functionalization and surface treatment of nanoparticles, American Scientific Publication, USA, 2003, 91.
4. Takacs. L., Self-sustaining reactions induced by ball milling, Progress in Material Science, 2002, 47(4), 355-414.
5. Alecu. I.D. and Stead. R.J., Development of forsterite ceramic materials at rojan advanced ceramics, Journal of the Australian Ceramic Society, 1998, 34(2), 50-53.
6. Kellar J.M., Symons W. and La Barge. W.J., Compound for a solid oxide fuel cell stack gasket, US Patent no. US7785725 B2 dated 31st Aug 2010, 1-8.
7. Ramesh S., Yaghoubi A., Sara Lee K.Y., Christopher Chin K.M., Purbolaksono J., Handi M. and Hassan M.A., Nanocrystalline Forsterite for Biomedical Applications: Synthesis, Microstructure and Mechanical Properties, J. Mech. Behav. Biomed. Mater., 2013, 25, 63-69.
8. Koike K., Chihara H., Koike C., Nakagawa M., Okada M., Tsuchiyama A., Aoki M., Awata T. and Atobe K,, Thermoluminescence of forsterite and fused quartz as a candidate for the extended red emission, Meteorit. Planet. Sci., 2002, 37, 1591-1598.
9. Willimason. G.K. and Hall. W.H., X-ray line broadening from filed aluminium and wolfram, Acta Metall., 1953, 1, 22-31.

10. Prabhu. Y.T., Rao. K.V., Sai Kumar. V.S., Kumari, B.S., Synthesis of ZnO Nanoparticles by a Novel Surfactant Assisted Amine Combustion Method, Advances in Nanoparticles, 2013, 2, 45-50.
11. Gualtieri A.F. and Bagni S., Crystal structure chemistry and color of doped-forsterites revisited by X-ray powder diffraction and UVNis/NIR spectroscopy, Per. Mineral., 2001 70, 27-56.
12. Holland. H.J. and Murtagh. M.J., An XRD morphology index for talcs: the effect of particle size and morphology on the specific surface area, Advances in X-ray Analysis, 2000, 42, 421-428.
13. Karthikeyan B., Rajamanickam N. and Bagare S.P., On the rotational temperature of AlH in sunspots, Sol. Phys., 2010, 64(2), 279-285.
14. Karthikeyan B., Rajamanickam N., Bagare S.P. and Raja V., On the search for BF, BH and BS molecular lines in sunspot spectra, Astropart. Phys., 2009, 31(1), 6-12.

*****